

The Supplement - Ice Composition

The focus of this investigation is the formation of formylphosphine (HCOPH_2), the simplest molecules containing a phosphorus peptide bond (-P-C(O)-) molecule, in defined laboratory simulation experiments. As model ice we choose the binary mixture of carbon monoxide (CO) and phosphine (PH_3) formed at temperatures around 5 K. While carbon monoxide has already been detected in interstellar ices with abundances to water of about 20%¹, up to now, phosphine has only been detected in the gas phase in circumstellar envelopes^{2, 3}. Nevertheless, it can be expected that upon ejection from circumstellar envelopes, where phosphine was detected, into the interstellar medium phosphine is incorporated into dense molecular clouds, where it subsequently condenses onto interstellar dust particle in icy mantles.

Supplement – Experimental procedure

The experiments were performed at the W. M. Keck Research Laboratory in Astrochemistry⁴⁻¹². The experimental setup consists of a steel ultra-high vacuum chamber (UHV) operated at a base pressure of a few 10^{-11} Torr. A polished silver wafer located within the chamber is coupled to a cold finger cooled to 5.5 ± 0.1 K using a UHV compatible closed-cycle helium compressor (Sumitomo Heavy Industries, RDK-415E). The target can be translated in the vertical axis and rotated in the horizontal plane. A gas mixture of phosphine (PH_3 , Sigma Aldrich; 99.9999 %) and carbon monoxide (CO, Matheson TriGas, 99.999 %) prepared in a gas mixing chamber at a ratio of 1:2 was deposited onto the cooled silver wafer via a glass capillary at a base pressure of 5.5×10^{-8} Torr for 20 min until the desired ice thickness was achieved. This ice growth was monitored online and in situ via interference pattern of a HeNe laser ($\lambda = 632.8$ nm; CVI Melles-Griot; 25-LHP-230) reflected from the silver wafer and the ice surface. The recorded fringes translate in an ice thickness via equation (1), which defines the thickness (d) of an ice and the dependence on the number of interference fringes (m), the laser wavelength (λ), and the angle of incidence of the laser beam ($\theta = 4^\circ$):¹³⁻¹⁶

$$d = \frac{m\lambda}{2\sqrt{n^2 - \sin^2 \theta}}. \quad (1)$$

With the weighted average refractive index (n) for phosphine (PH_3) ice of 1.40 ± 0.30 and carbon monoxide (CO) ice of 1.25 ± 0.03 ,¹⁷ a thickness of 700 ± 100 nm is determined. Based on the integration of the adsorption features and their absorption strength A for

phosphine (PH_3 , 982 cm^{-1} $A = 5.1 \times 10^{-17} \text{ cm molecule}^{-1}$)¹⁸ and carbon monoxide (CO , 2138 cm^{-1} $A = 1.6 \times 10^{-17} \text{ cm molecule}^{-1}$)¹⁷ we determined their ratio $\text{PH}_3:\text{CO} = 1:2 \pm 0.5$ within the ice. After the deposition, an area of $1.0 \pm 0.1 \text{ cm}^2$ of the ice mixture was irradiated with 5 keV electrons for 15 min with an electron current of 20 nA at an angle of incidence of 70° relative to the surface normal. Galactic cosmic rays interacting with interstellar ices consisting mainly of protons with kinetic energy up to GeV. An interaction of these GCRs with solids generates a cascade of secondary electrons with energies in the range from a few eV up to keV¹⁹⁻²¹. Therefore, the 5 keV electrons mimic efficiently the irradiation by GCR induced electron cascades. By utilizing CASINO 2.42 software²² an average penetration depth of $240 \pm 80 \text{ nm}$ is calculated (Table S2). The average dose absorbed is determined to be $0.8 \pm 0.2 \text{ eV molecule}^{-1}$ and $0.6 \pm 0.1 \text{ eV molecule}^{-1}$ for phosphine and carbon monoxide, respectively. During the irradiation the chemical evolution of the ice mixture was monitored online and in situ using FTIR (Nicolet 6700, MCT-A) in the range of $4500 \text{ cm}^{-1} - 500 \text{ cm}^{-1}$, with a resolution of 4 cm^{-1} , at a reflection angle of 45° for absorption-reflection-absorption mode. Once the irradiation is complete, the ice was held isothermally at 5.5 K for additional 30 min before starting temperature programmed desorption (TPD) by heating the substrate from 5.5 K to 320 K at a rate of 1 K min^{-1} . Note that throughout the TPD process, the subliming molecules were detected via QMS (Extrel, Model 5221) operating in residual gas analyzer (RGA) mode operating with electron impact ionizer of 100 eV, an emission current of 1 mA, and a mass range up to 500 amu.

To detect the subliming molecules with the isomer-selective PI-ReTOF-MS approach, the neutral molecules subliming in the temperature programmed desorption phase are ionized by pulsed vacuum ultraviolet (VUV) laser light close to 2 mm in front of the ice sample. The ions produced are mass-resolved and detected by a multichannel plate in a dual chevron configuration and then amplified by a fast preamplifier (Ortec 9305) and shaped with a 100 MHz discriminator. Finally, the spectra are recorded using a personal-computer-based multichannel scaler (FAST ComTec, P7888-1E) with 4 ns bin widths triggered at 30 Hz using a pulse delay generator (Quantum Composer, 9518) and 3600 sweeps per mass spectrum per 1 K increase in temperature during TPD. The experiments were taken out at different photoionization energies and additionally with C^{18}O (Sigma Aldrich; 95 % ^{18}O , 99.9% ^{12}C) and ^{13}CO (Sigma Aldrich, <5% ^{18}O , 99% ^{13}C) to verify the composition of a desorbing molecule via isotopic mass shift.

The VUV light is generated by difference-frequency mixing ($2\omega_1 - \omega_2$) in a noble gas (krypton (Kr) and xenon (Xe)) using two dye lasers (Sirah Lasertechnik, Model Cobra-Stretch, and Precision Scan) each pumped by a Nd:YAG laser (Spectra-Physics, Models PRO-270-30). In order to record and monitor the VUV light a detection system consisting of a Faraday cup and a diode calibrated by the national institute of standards and technology (NIST) is placed behind the detection region. This tunable VUV photon source allows soft-ionization of molecules with ideally no fragmentation²³⁻²⁷. In this work we used the third harmonic of the Nd:YAG laser in order to generate the third harmonic of 355 nm in xenon gas with a photon energy of 10.49 eV. For the second energy we used Coumarin 503 as dye pumped by 355 nm to achieve $\omega_1 = 445.132$ nm which is doubled to 222.566 nm. Mixed in xenon with 733 nm generated from LDS 722 pumped by 532 nm results 9.67 eV. Finally, we used a mixture of Rhodamin 610 and Rhodamine 640 in the first dye laser, pumped by 532 nm, to generate 606.948 nm, which is frequency tripled to $\omega_1 = 202.316$ nm for the two-photon resonance of krypton (Kr). Adding the second dye laser with Coumarin 480 pumped by 355 nm with an output wavelength of $\omega_2 = 485$ nm results in the VUV energy of 9.45 eV. Table S4 presents an overview of all photon energies used. Note that calibration data for the ReTOF reveal a lowering of the ionization energies of the subliming molecules by up to 0.03 to 0.04 eV due to the static electric field induced Stark shift⁸.

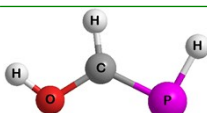
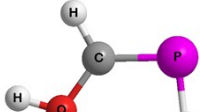
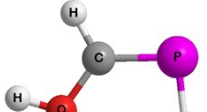
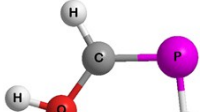
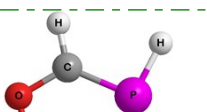
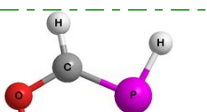
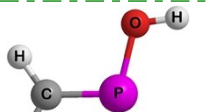
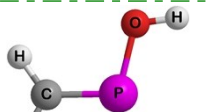
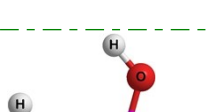
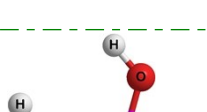
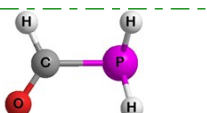
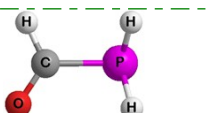
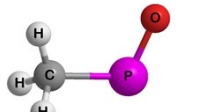
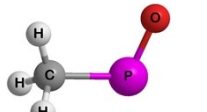
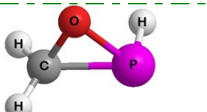
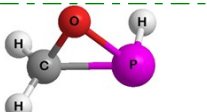
Supplement - Theoretical calculation

The hybrid density functional B3LYP²⁸⁻³¹ with the cc-pVTZ basis set was employed to optimize geometries and harmonic frequencies of the species and their cations. Their coupled cluster³²⁻³⁵ CCSD(T)/cc-pVDZ, CCSD(T)/ccpVTZ, and CCSD(T)/cc-pVQZ energies were calculated and extrapolated to complete basis set limits,³⁶ CCSD(T)/CBS, with B3LYP/cc-pVTZ zero-point energy corrections. The energy difference between the ionic and neutral state with similar geometry gives the adiabatic ionization energy. The potential energy curve for HCO + PH₂ → HCOPH₂ or its reverse HCOPH₂ → HCO + PH₂ reaction along the reaction coordinate C -- P distance is obtained with intrinsic reaction coordinate (IRC) calculations at B3LYP/cc-pVTZ level of theory. The GAUSSIAN09 program³⁷ was utilized in the electronic structure calculations. A variational transition state for this reaction at total energy of 250 kJ/mol is located by facilitating variational RRKM theory. A comparison with

literature data of known ionization energies with theoretical values suggests that the calculations overestimate the ionization energies typically by 0.03 eV to 0.05 eV³⁸⁻⁴¹

The electronic structure calculations reveal the existence of five closed shell structural isomers (**I-V**) along with three cis-trans isomers (**I'**, **I''**, **II'**), whose adiabatic ionization energies and relative energies are presented in Fig. 1. Methyloxophosphine (CH_3PO ; **IV**) represents the global minimum with methylene phosphinous acid (**II**, **II'**) being less stable by 0.20 to 0.21 eV followed by PCA (HCOPH_2 ; **III**; + 0.81 eV) and the nearly isoenergetic phosphinidene methanol (HPCH(OH) ; **I**, **I'**, **I''**; +1.05 to +1.14 eV) and oxaphosphirane (c- CH_2PHO ; **V**; +1.11 eV) isomers.

Table S1 The adiabatic ionization energies (IE) and relative energies (ΔE) of formylphosphine and its isomers.

	B3LYP/ cc-pVTZ + E _{zpc} ^a	E _{zpc} ^b	CCSD(T)/ CBS	IP(eV) ^c	E(eV) ^d
	I -456.484403	0.039259	-455.908717	0.00	1.14
	I⁺ -456.165889	0.038639	-455.580778	8.91	10.04
	I' -456.485307	0.039237	-455.909089	0.00	1.13
	I'⁺ -456.165326	0.038949	-455.580384	8.94	10.06
	I'' -456.488198	0.039641	-455.912440	0.00	1.05
	I''⁺ -456.164247	0.038774	-455.579719	9.03	10.08
	II -456.514976	0.039381	-455.942955	0.00	0.21
	II⁺ -456.182633	0.039020	-455.601415	9.28	9.49
	II' -456.514978	0.039679	-455.943472	0.00	0.20
	II''⁺ -456.177995	0.038400	-455.596567	9.40	9.61
	III -456.499392	0.035452	-455.916934	0.00	0.81
	III⁺ -456.153935	0.034229	-455.561947	9.63	10.44
	IV -456.522252	0.039001	-455.950255	0.00	0.00
	IV⁺ -456.175693	0.038520	-455.595359	9.64	9.64
	V -456.483339	0.039237	-455.909838	0.00	1.11
	V⁺ -456.130319	0.037828	-455.548528	9.79	10.90

^a B3LYP/cc-pVTZ energy with zero-point energy correction in hartree.

^b zero-point energy by B3LYP/cc-pVTZ in hartree.

^c relative ionization potential by CCSD(T)/CBS with B3LYP/cc-pVTZ zero-point energy correction in eV.

^d the relative energy of different isomer sets in eV

Table S2 Data applied to calculate the irradiation dose per molecule. * values from CASINO simulations, \$ derived values based on 20 nA, 15 min irradiation of ice mixtures containing phosphine(PH_3) and carbon monoxide (CO)

initial kinetic energy of the electrons, E_{init}	5 keV
irradiation current, I	$20 \pm 2 \text{ nA}$
total number of electrons	$(1.5 \pm 0.3) \times 10^{14}$
average kinetic energy of backscattered electrons, E_{bs}^*	$3.54 \pm 0.30 \text{ keV}$
fraction of backscattered electrons, f_{bs}^*	0.4 ± 0.1
average kinetic energy of transmitted electrons, E_{trans}^* ,	$2.9 \pm 0.3 \text{ keV}$
fraction of transmitted electrons, f_{trans}^*	0
average penetration depth, l*	$240 \pm 80 \text{ nm}$
density of the ice, ρ	$1.2 \pm 0.1 \text{ g cm}^{-3}$
irradiated area, A	$1.0 \pm 0.1 \text{ cm}^2$
total number of molecules processed\$	$(4 \pm 1) \times 10^{17}$
dose per molecule PH_3 , $D^{\$}$	$0.8 \pm 0.2 \text{ eV}$
dose per molecule CO, $D^{\$}$	$0.6 \pm 0.1 \text{ eV}$

Table S3 Infrared absorption features of phosphine (PH_3)^{16, 18} and the carbon monoxide (CO , ^{13}CO , and C^{18}O)^{17, 42, 43}

Wavenumber / cm^{-1}	Vibration mode	Assignment
PH ₃ contribution		
3407	PH ₃	$\nu_1 + \nu_4$
3300	PH ₃	$\nu_1 + \nu_2$
2435	PH ₃	$\nu_1 + \nu_L$
2203	PH ₃	$\nu_2 + \nu_4$
1103	PH ₃	ν_4
986	PH ₃	ν_2
$\text{CO}, ^{13}\text{CO}, \text{C}^{18}\text{O}$ contribution		
2136	CO stretching	ν_1
2091	^{13}CO stretching	$\nu_1(^{13}\text{CO})$
2088	C^{18}O stretching	$\nu_1(\text{C}^{18}\text{O})$
processed ice		
2350	CO_2	$\nu_3 (\text{CO}_2)$
2044	$^{13}\text{C}^{18}\text{O}$	$\nu_1(^{13}\text{C}^{18}\text{O})$
2000	C_2O	$\nu_1 (\text{C}_2\text{O})$
1059	P_2H_4	$\nu_3 (\text{P}_2\text{H}_4)$

Table S4 Parameter for the vacuum ultraviolet light generation used in the present experiments.

	Photoionization energy / eV	10.49	9.67	9.45
	Flux (10^{11} photons s $^{-1}$)	13nA	30nA	10nA
$(2\omega_1 - \omega_2)$	Wavelength / nm	118.2	128.2	131.2
ω_1	Wavelength / nm	355	111.283	202.316
Nd:YAG (ω_1)	Wavelength / nm	355	355	532
Dye laser (ω_1)	Wavelength / nm - dye laser	-	222.566	606.948
Dye		-	C 503	Rh 610/Rh 640
ω_2	Wavelength / nm	-	733	485
Nd:YAG (ω_1)	Wavelength / nm - Nd:YAG	-	532	355
Dye laser (ω_1)	Wavelength / nm - dye laser	-	733	485
Dye		-	LDS 722	C 480
	Nonlinear medium	Xe	Xe	Kr

Table S5 Computational results for the formation of HCOPH₂

	B3LYP/ cc-pVTZ + E _{zpc} ^a	E _{zpc} ^b	CCSD(T)/ CBS	E(kJ/mol) ^c
CO(C_{∞v}, ¹Σ⁺)	-113.352214	0.005039	-113.206290	
HCO(C_s, ²A')	-113.885942	0.012946	-113.736916	
PH₂(C_{2v}, ²B₁)	-342.527852	0.013342	-342.076968	
PH₃(C_{3v}, ¹A₁)	-343.156117	0.023847	-342.716534	
HCOPH₂(C₁, ¹A)	-456.499392	0.035452	-455.916934	0.0
ts-HCO+PH₂-V^d	-456.419355	0.028223	-455.819099	237.9
HCO+PH₂	-456.413794	0.026288	-455.813884	246.5
ts-CO+PH₃	-456.410338	0.029204	-455.818367	242.4
CO+PH₃	-456.508331	0.028886	-455.922825	-32.7

^a B3LYP/cc-pVTZ energy with zero-point energy correction in hartree.

^b zero-point energy by B3LYP/cc-pVTZ in hartree.

^c relative energy by CCSD(T)/CBS with B3LYP/cc-pVTZ zero-point energy correction in kJ/mol.

^d the variational transition state found at collision energy 250.0 kJ/mol.

Table S6 B3LYP/cc-pVTZ optimized structures of the PH₃CO isomers and their ions PH₃CO⁺.

Atom	X	Y	Z	Atom	X	Y	Z
CH₃PO				CH₃PO⁺			
P	0.251382	-0.509100	0.000007	P	0.239701	-0.461586	-0.000003
O	1.262572	0.587635	0.000000	O	1.328543	0.516834	0.000002
C	-1.426208	0.282213	0.000062	C	-1.493908	0.266129	-0.000005
H	-1.981691	-0.064670	0.877037	H	-1.529766	0.875899	0.907993
H	-1.979814	-0.061469	-0.879429	H	-2.201024	-0.559906	-0.000231
H	-1.352557	1.368273	0.001910	H	-1.529621	0.876338	-0.907708
Atom	X	Y	Z	Atom	X	Y	Z
H₂CPOH				H₂CPOH⁺			
H	2.316238	0.134131	0.000000	H	2.356637	-0.154581	0.000000
H	1.374354	-1.459763	0.000000	H	1.248271	-1.636980	0.000000
C	1.363158	-0.377628	0.000000	C	1.346178	-0.554620	0.000000
P	0.000000	0.551696	0.000000	P	0.000000	0.589857	0.000000
O	-1.223781	-0.569309	0.000000	O	-1.298267	-0.306159	0.000000
H	-2.079287	-0.129564	0.000000	H	-1.295840	-1.279307	0.000000
Atom	X	Y	Z	Atom	X	Y	Z
H₂CPOH'				H₂CPOH'⁺			
H	-2.310319	0.003522	0.000125	H	-2.360875	-0.052525	-0.000501
H	-1.295561	1.538608	0.000193	H	-1.333282	1.504638	-0.000242
C	-1.326051	0.454811	0.000109	C	-1.383514	0.419641	0.000154
P	-0.022982	-0.564819	-0.000043	P	0.053625	-0.590024	-0.000002

O	1.340437	0.361035	-0.000046	O	1.139627	0.572806	-0.000012
H	1.183420	1.313012	0.000039	H	2.073852	0.297944	-0.000055
Atom	X	Y	Z	Atom	X	Y	Z
HCOPH₂				HCOPH₂⁺			
C	-0.730343	0.434300	0.011436	C	-0.820207	0.503041	-0.038654
H	-0.889640	1.533818	0.002710	H	-1.084913	1.569881	-0.080527
O	-1.656276	-0.330212	0.009917	O	-1.084913	-0.420931	0.054300
H	1.068243	-0.071981	-0.116699	H	1.060956	-0.006824	-0.087796
P	1.529280	0.804822	0.898919	P	1.482229	0.298318	1.230249
H	0.968984	-1.223034	0.700904	H	0.953478	-1.416632	-0.035255
Atom	X	Y	Z	Atom	X	Y	Z
HPCH(OH)				HPCH(OH)⁺			
C	0.459302	0.457120	-0.000020	C	0.544308	0.486386	-0.000161
H	0.656747	1.524878	-0.000029	H	0.777499	1.550911	-0.000818
O	1.560024	-0.329878	-0.000019	O	1.517350	-0.349001	0.000209
P	2.356395	0.209714	0.000188	P	2.406854	0.054899	-0.000058
H	-1.102473	-0.195291	0.000006	H	-1.125826	-0.189580	-0.000109
H	-1.712054	1.091073	0.000024	H	-1.701608	1.111583	0.001813
Atom	X	Y	Z	Atom	X	Y	Z
HPCH(OH)'				HPCH(OH)'⁺			
C	0.46375000	0.46008900	-0.00005000	C	0.54831100	0.48982600	-0.00005100
H	0.68447300	1.52541400	0.00000100	H	0.80366700	1.55003300	0.00011500
O	1.54773900	-0.34748600	0.00005700	O	1.50565700	-0.36266200	0.00000200
H	2.35563000	0.17730100	0.00011600	H	2.40201600	0.02869800	0.00006900

P	-1.15465600	-0.01761800	-0.00001800	P	-1.17952900	-0.01442300	0.00000600
H	-0.88467600	-1.41909200	-0.00000100	H	-0.84787100	-1.40005300	0.00001500
Atom	X	Y	Z	Atom	X	Y	Z
HPCH(OH)"				HPCH(OH)"⁺			
C	-0.46301700	0.49591800	0.00000200	C	0.54919100	0.50494700	0.00013300
H	-0.64761400	1.56346600	0.00003000	H	0.76035400	1.57264500	-0.00051600
O	-1.63300800	-0.17117500	0.00003000	O	1.61792600	-0.19656900	-0.00002400
H	-1.47268000	-1.12498000	0.00002200	H	1.48857500	-1.16676600	0.00015800
P	1.08037500	-0.20590100	-0.00002000	P	-1.11753800	-0.19676300	-0.00004300
H	1.75684100	1.04392400	-0.00000400	H	-1.72442100	1.08842500	0.00039300
Atom	X	Y	Z	Atom	X	Y	Z
c-H₂CPHO				c-H₂CPHO⁺			
C	-0.944128	-0.539172	0.002395	C	-1.048285	-0.456242	-0.075394
P	0.813570	-0.095629	0.107750	P	0.776432	-0.188196	0.083874
O	-0.607016	0.842776	-0.041070	O	-0.482430	0.857514	0.056562
H	-1.449358	-0.859728	0.907610	H	-1.440784	-0.899778	0.833890
H	-1.342031	-0.940198	-0.924027	H	-1.555050	-0.633571	-1.016449
H	1.108729	-0.272810	-1.285643	H	1.498503	0.233631	-1.075683

Table S7 B3LYP/cc-pVTZ calculated vibrational modes of the PH₃CO isomers and their ions PH₃CO⁺.

HPCH(OH)

Normal modes	Vibration mode	Frequency(cm ⁻¹)	IR Intensity
v1	HPOH twisting	352.2824	107.65
v2	PCO scissoring	389.4706	1.7169
v3	HPOH wagging	594.4738	10.468
v4	HP-CH scissoring + HC-OH rocking	841.3531	3.5445
v5	HP-CH twisting	860.5178	26.5837
v6	HP-CH rocking + HC-OH rocking	957.4146	63.9629
v7	HP-CH scissoring + CO stretching + HC-OH rocking	1219.0186	352.3106
v8	HC-OH scissoring	1241.5906	33.3513
v9	HC-OH rocking	1471.5584	51.9688
v10	HP stretching	2359.8667	77.5568
v11	CH stretching	3124.5871	10.9221
v12	OH stretching	3820.521	126.9196

HPCH(OH)⁺

Normal modes	Vibration mode	Frequency(cm ⁻¹)	IR Intensity
v1	HP-CH twisting	116.1091	0.002
v2	PCO scissoring	367.4615	1.9713
v3	HP-CH wagging + HC-OH wagging	610.327	119.611
v4	HP-CH stretching + HC-OH rocking	722.061	13.5387
v5	HPOH rocking	938.4938	63.8354
v6	HC-OH twisting	960.8188	11.2865
v7	HC-OH scissoring	1226.6691	63.6294
v8	HCO scissoring + HC-OH rocking	1369.5022	178.6769
v9	HC-OH rocking + COH scissoring	1503.5909	117.2882
v10	HP stretching	2390.9625	5.3614
v11	CH stretching	3117.1008	8.8414
v12	OH stretching	3637.5894	400.3086

HPCH(OH)'

Normal modes	Vibration mode	Frequency(cm ⁻¹)	IR Intensity
v1	HPC rocking	387.3848	5.9197
v2	HP-COH wagging	392.2617	122.2181
v3	HP-COH twisting	581.9135	3.0746
v4	HP-CH rocking	805.6662	7.0298
v5	HP-CH wagging	899.0557	18.0601
v6	HP-COH rocking	940.403	52.9969
v7	HC-OH rocking + CO stretching	1217.0313	308.3518
v8	HC-OH scissoring	1261.2518	29.3562
v9	HC-OH rocking + CO stretching	1489.8716	50.8908
v10	PH stretching	2344.1136	66.5447
v11	CH stretching	3108.956	13.3931
v12	OH stretching	3795.0531	95.6642

HPCH(OH)⁺

Normal modes	Vibration mode	Frequency(cm ⁻¹)	IR Intensity
v1	PH wagging	234.2508	9.4677
v2	CPH rocking	381.3453	9.0861
v3	HC-OH wagging	618.6653	134.7069
v4	CP stretching	698.225	15.0041
v5	HP rocking	931.6661	60.6574
v6	HC-OH twisting	987.5646	5.2536
v7	HC-OH scissoring	1244.6311	51.5742
v8	HC-OH rocking + CO stretching	1365.5181	188.4679
v9	CO stretching + HC-OH rocking	1518.6644	84.8632
v10	PH stretching	2386.1154	3.839
v11	CH stretching	3113.0637	7.6529
v12	OH stretching	3616.8534	355.1399

HPCH(OH)"

Normal modes	Vibration mode	Frequency(cm ⁻¹)	IR Intensity
v1	HPC-OH scissoring	385.2988	14.6627
v2	HPC-OH wagging	497.9217	52.6045
v3	HPC-OH twisting	607.7955	16.3906
v4	HP-CH scissoring	825.2449	22.2881
v5	HC-OH wagging	907.062	65.4191
v6	HP rocking + HO rocking	952.9297	3.0471
v7	HC-OH rocking	1202.7695	265.1447
v8	COH scissoring	1291.4906	70.5476
v9	HO-CH rocking	1451.2408	151.7648
v10	PH stretching	2374.277	62.0805
v11	CH stretching	3165.5089	3.6335
v12	OH stretching	3738.9332	41.407

HPCH(OH)^{''+}

Normal modes	Vibration mode	Frequency(cm ⁻¹)	IR Intensity
v1	HP-CH twisting + HC-OH twisting	128.6902	19.0375
v2	HP-CH scissoring + COH rocking	358.3523	14.0267
v3	HC-OH twisting	638.9878	57.0222
v4	HC-PH scissoring + CP stretching	708.6132	10.0293
v5	PH rocking	925.5392	6.7644
v6	HC-OH wagging	1002.7374	82.6486
v7	HC-OH rocking	1218.998	217.9689
v8	HC-OH scissoring	1418.214	0.108
v9	CH rocking + OC stretching	1478.0049	232.2284
v10	PH stretching	2398.3343	1.4325
v11	CH stretching	3141.0696	16.2622
v12	OH stretching	3602.393	182.6903

HCOPH₂⁺

Normal modes	Vibration mode	Frequency(cm ⁻¹)	IR Intensity
v1	HPH rocking + HC-PH twisting	136.7327	17.5203
v2	CO-PH scissoring	309.8804	2.0692
v3	HC-PH scissoring	499.3164	49.6413
v4	HPH wagging + HP-CH rocking	542.6962	149.8602
v5	HPH twisting	723.6532	2.9964
v6	HC-PH twisting	878.859	34.5654
v7	HPH scissoring	1059.6461	29.9883
v8	HC-PH scissoring	1192.7929	19.5155
v9	CO stretching	1814.9783	57.458
v10	HPH symmetric stretching	2411.382	4.7081
v11	HPH asymmetric stretching	2447.0951	3.5064
v12	HC stretching	3007.6449	42.6548

HCOPH₂

Normal modes	Vibration mode	Frequency(cm ⁻¹)	IR Intensity
v1	HC-PH twisting + HPH rocking	194.0925	7.9222
v2	HCO rocking + HC-PH scissoring + HPH rocking	358.2837	7.9852
v3	HC-PH scissoring + HPH twisting	581.6857	42.91
v4	HC-PH scissoring + HPH wagging	664.3063	3.8511
v5	HPH twisting	872.6129	36.8003
v6	HC-PH twisting + HPH wagging	966.4531	14.0842
v7	HPH scissoring	1103.2446	18.4707
v8	HC rocking	1384.9569	20.7183
v9	CO stretching	1771.8525	262.506
v10	HPH symmetric stretching	2394.6705	34.669
v11	HPH symmetric stretching	2424.4483	28.161
v12	HC stretching	2845.2063	127.8406

c-H₂CPHO⁺

Normal modes	Vibration mode	Frequency(cm ⁻¹)	IR Intensity
v1	HO-PH wagging	626.9262	10.013
v2	PH scissoring	682.5188	20.6917
v3	HC-PH twisting + HCH rocking	714.7449	23.2655
v4	HCH twisting	868.2192	0.3929
v5	HP0-CH wagging	987.4089	19.023
v6	CO symmetric stretching + HCH wagging	1054.1656	14.3303
v7	HCH wagging	1126.7616	22.4394
v8	HCH rocking	1142.4538	1.9696
v9	HCH scissoring	1492.6492	1.204
v10	HP stretching	2275.3522	141.1797
v11	HCH symmetric stretching	3080.9607	19.4491
v12	HCH asymmetric stretching	3171.0469	12.1746

c-H₂CPHO

Normal modes	Vibration mode	Frequency(cm ⁻¹)	IR Intensity
v1	OPC scissoring+OPH rocking	244.3218	62.8467
v2	HP-CH rocking	658.5863	2.9791
v3	PH-CH scissoring	698.5228	6.2827
v4	HCH twisting + HP-CH scissoring	795.6271	15.7614
v5	HP-CH rocking + HCH rocking	841.04	42.509
v6	HCH wagging	1043.7645	11.1925
v7	HCH wagging	1094.5309	49.2932
v8	HCH rocking	1115.9591	1.3125
v9	HCH scissoring	1473.9062	1.6821
v10	HP stretching	2298.3629	18.7423
v11	HCH symmetric strerching	3105.4437	20.3337
v12	HCH asymmetric strerching	3234.5642	23.0361

CH₃PO

Normal modes	Vibration mode	Frequency(cm ⁻¹)	IR Intensity
v1	2 × CH rocking	44.47	0.2109
v2	C-H H-C-H rocking + O-H scissoring	337.50	13.0766
v3	CP symmetric stretching	635.79	51.3316
v4	2 × CH out-of-plane twisting	693.08	0.1129
v5	C-H H-C-H out-of-plane wagging	845.15	28.0682
v6	OP in-plane scissoring	1219.34	76.4014
v7	C-H H-C-H out-of-plane wagging	1276.49	28.5871
v8	2 × CH rocking	1434.45	14.9847
v9	2 × CH scissoring	1435.38	10.1932
v10	3 × CH symmetric stretching	3003.56	0.5602
v11	2 × CH asymmetric stretching	3066.47	4.3021
v12	2 × CH symmetric stretching + C-H scissoring	3127.77	2.4617

CH₃PO⁺

Normal modes	Vibration mode	Frequency(cm ⁻¹)	IR Intensity
v1	C-H H-C-H rocking	31.57	3.2240
v2	C-P out-of-plane twisting + O C-H in-plane scissoring	248.96	17.3559
v3	CH ₃ -P scissoring	482.86	2.1156
v4	C-H H-C-H out-of-plane twisting	734.03	1.2600
v5	2 × CH out-of-plane twisting + 2 × CH out-of-plane wagging	856.41	5.9046
v6	3× CH out-of-plane wagging	1214.91	2.7393
v7	O-P scissoring + 3× CH out-of-plane wagging	1286.62	6.5438
v8	2 × CH in-plane scissoring	1374.11	18.5535
v9	2 × CH in-plane scissoring + 2×CH rocking	1404.78	16.7795
v10	3×CH symmetric stretching	3002.97	63.4081
v11	2×CH asymmetric stretching	3103.75	34.6882
v12	2×CH symmetric stretching + C-H stretching	3167.19	22.2162

H₂CPOH(Cs)

Normal modes	Vibration mode	Frequency(cm ⁻¹)	IR Intensity
v1	O-H out-of-plane wagging	327.63	92.0840
v2	O-H C-H scissoring + 2 × CH rocking	332.46	0.8952
v3	2 × CH out-of-plane twisting + O-H C-H out-of-plane wagging + O-H C-H out-of-plane twisting	649.16	0.0000
v4	2 × CH rocking + O-H rocking	766.68	71.1216
v5	2 × CH out-of-plane wagging	792.95	92.5434
v6	2 × CH rocking + OH P scissoring	830.64	65.6812
v7	O-H C-H scissoring + CH ₂ P scissoring	1003.72	68.5265
v8	OH P scissoring	1084.46	75.7502
v9	2 × CH scissoring	1412.96	16.6458
v10	2 × CH symmetric stretching	3138.33	0.0103
v11	2 × CH asymmetric stretching	3235.93	0.0854
v12	O-H scissoring	3842.27	127.2661

H₂CPOH⁺(Cs)

Normal modes	Vibration mode	Frequency(cm ⁻¹)	IR Intensity
v1	2 × CH out-of-plane twisting	240.43	4.7111
v2	OH CH ₂ in-plane scissoring	334.38	7.6706
v3	OH CH out-of-plane twisting	541.69	133.2675
v4	2 × CH rocking + OH CH rocking	778.41	5.4258
v5	OH CH ₂ out-of-plane wagging	804.77	62.0083
v6	OH CH rocking	822.33	56.7731
v7	O-H rocking + OH CH scissoring + 2 × CH rocking	905.19	183.9227
v8	OH CH scissoring + 2 × CH rocking	1012.09	10.1378
v9	2 × CH scissoring	1413.89	18.5038
v10	2 × CH symmetric stretching	3101.52	33.5814
v11	2 × CH asymmetric stretching	3211.78	20.7958
v12	O-H scissoring	3689.29	210.9594

H₂CPOH'

Normal modes	Vibration mode	Frequency(cm ⁻¹)	IR Intensity
v1	2 × CH rocking + CH OH scissoring	339.63	14.7860
v2	CH OH out-of-plane twisting	625.34	101.7505
v3	2 × CH out-of-plane twisting	626.32	14.5435
v4	2 × CH rocking + CH OH rocking	772.13	16.1493
v5	2 × CH out-of-plane wagging	780.38	73.6443
v6	2 × CH rocking + CH OH rocking	823.79	169.4213
v7	CH ₂ P scissoring + OH CH ₂ rocking	994.72	1.2433
v8	CH OH scissoring	1045.69	59.2939
v9	2 × CH scissoring	1420.85	17.5528
v10	2× CH symmetric stretching	3120.29	2.2198
v11	2× CH asymmetric stretching	3213.73	1.4100
v12	OH scissoring	3783.56	33.9048

H₂CPOH⁺

Normal modes	Vibration mode	Frequency(cm ⁻¹)	IR Intensity
v1	2 × CH out-of-plane twisting	314.39	1.5921
v2	OH CH scissoring + 2 ×CH scissoring	341.09	5.6955
v3	OH CH out-of-plane wagging	592.11	127.0052
v4	2 × CH rocking	804.89	1.5976
v5	2 × CH out-of-plane wagging	825.79	6.1184
v6	2 × CH rocking + OH CH rocking	846.50	37.9733
v7	OP scissoring + 2 × CH rocking + OH CH scissoring	942.08	105.8477
v8	OH P scissoring + CH OP rocking	1021.68	106.5002
v9	2 × CH scissoring	1402.11	18.1969
v10	2 × CH symmetric stretching	3110.92	38.9800
v11	2 × CH asymmetric stretching	3228.78	28.8960
v12	OH scissoring	3697.44	389.7698

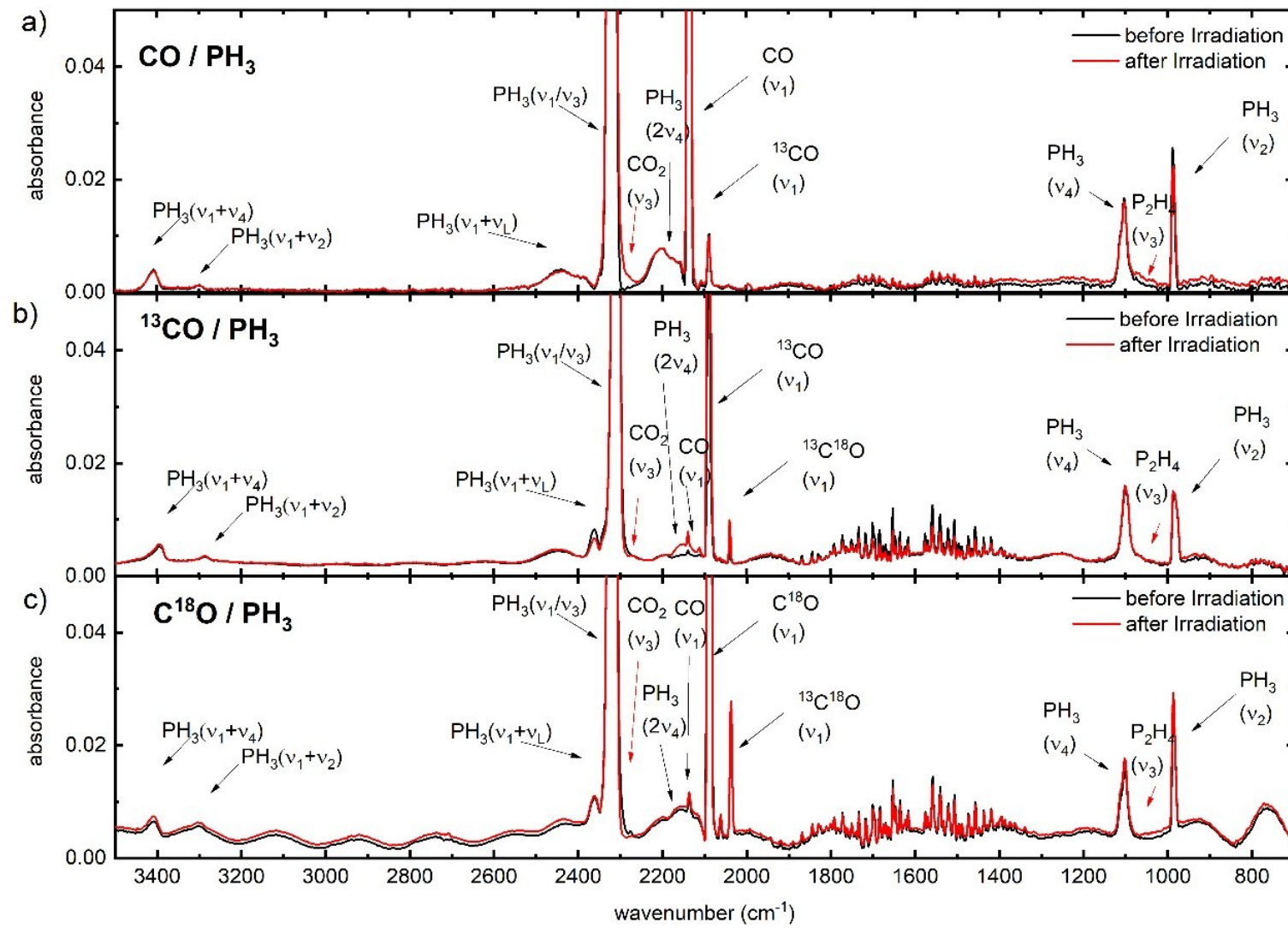


Fig. S1 FTIR spectra before (black) and after (red) the irradiation of the phosphine (PH₃) - carbon monoxide (CO) (a), the ^{¹³}C-isotope (^{¹³}CO) (b) and the ^{¹⁸}O-Isotope (C^{¹⁸}O) (c) ice mixtures.

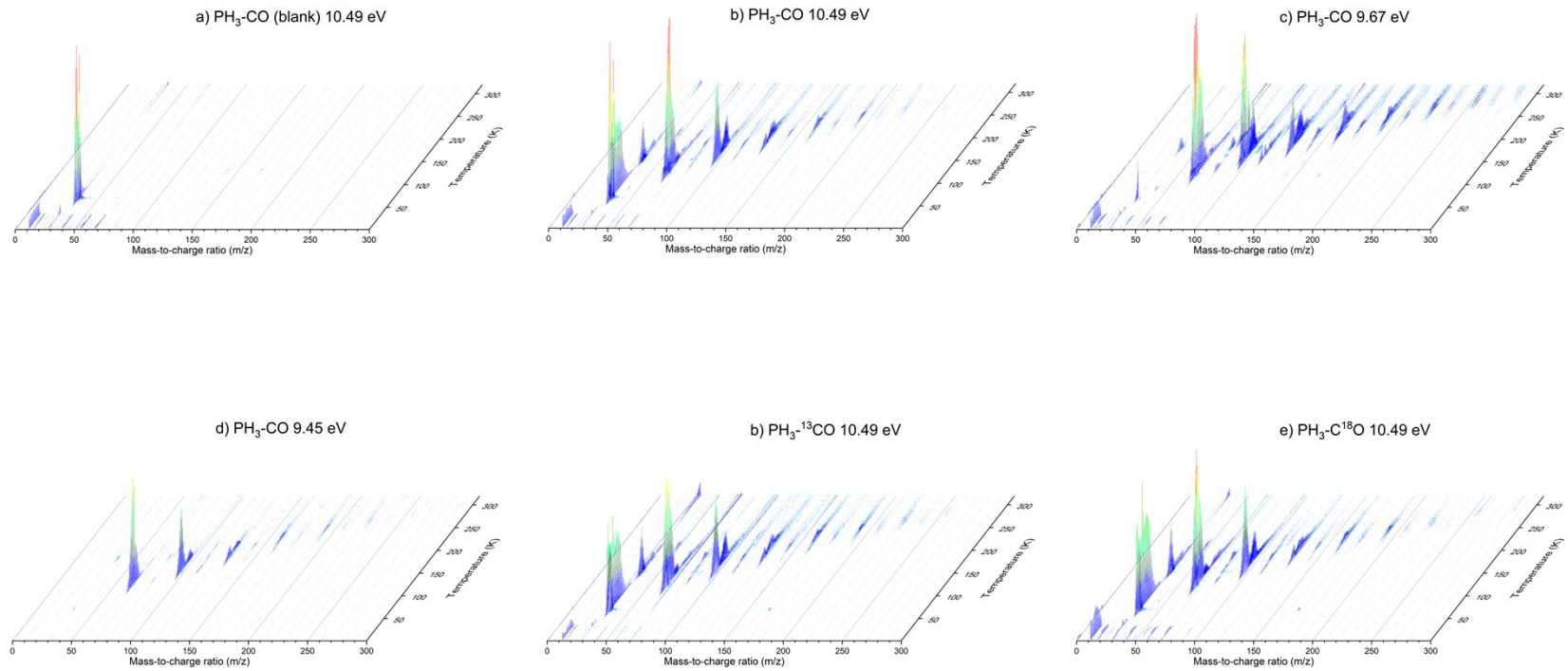


Fig S2 PI-ReTOF-MS spectra of the subliming molecules recorded at distinct ionization energies for the irradiated ice mixtures containing phosphine (PH_3) and carbon monoxide (CO) and its isotopic counterparts (C^{18}O ; ^{13}CO). Panel (a) and (b) show the non-irradiated ice mixture (PH_3/CO) (blank) and the irradiated (20nA 15min). Panel (c) and (d) show identical ice mixtures at lower ionization energies. In (d) and (e) are ice mixtures of the isotopic counterparts $\text{C}^{13}\text{-carbonmonoxide}$ and $\text{O}^{18}\text{-carbonmonoxide}$.

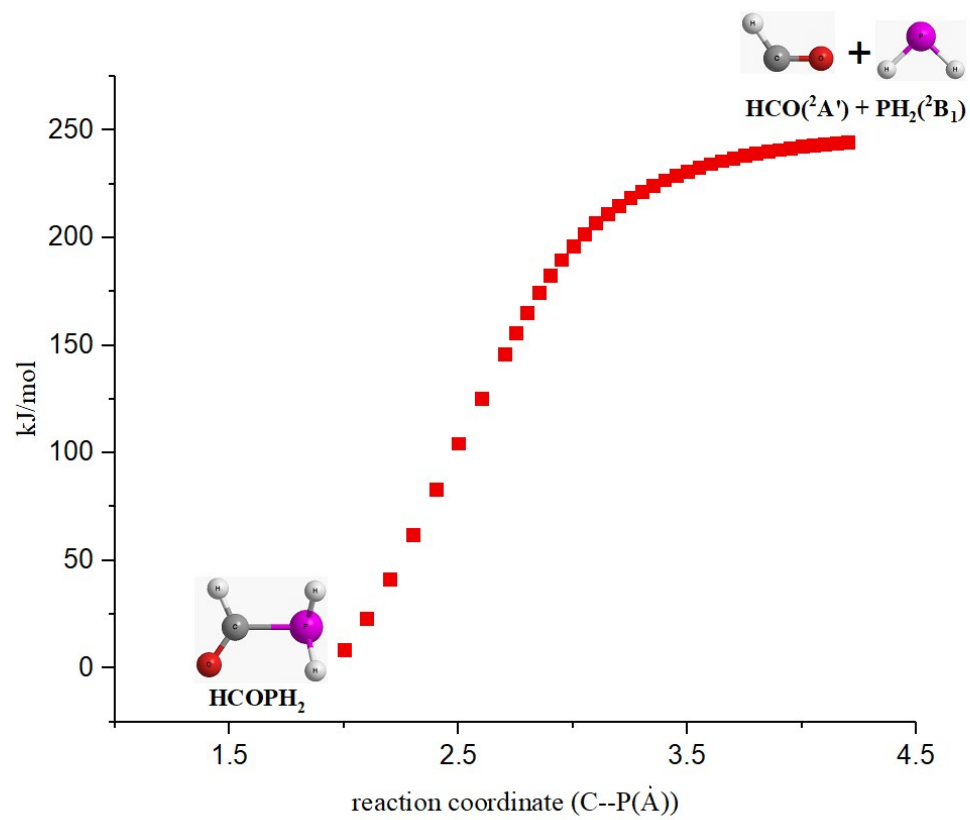


Fig. S3 The potential energy curve for $\text{HCO} + \text{PH}_2 \rightarrow \text{HCOPH}_2$ reaction along reaction coordinate (C--P) obtained with IRC (intrinsic reaction coordinate) calculation at B3LYP/cc-pVTZ level.

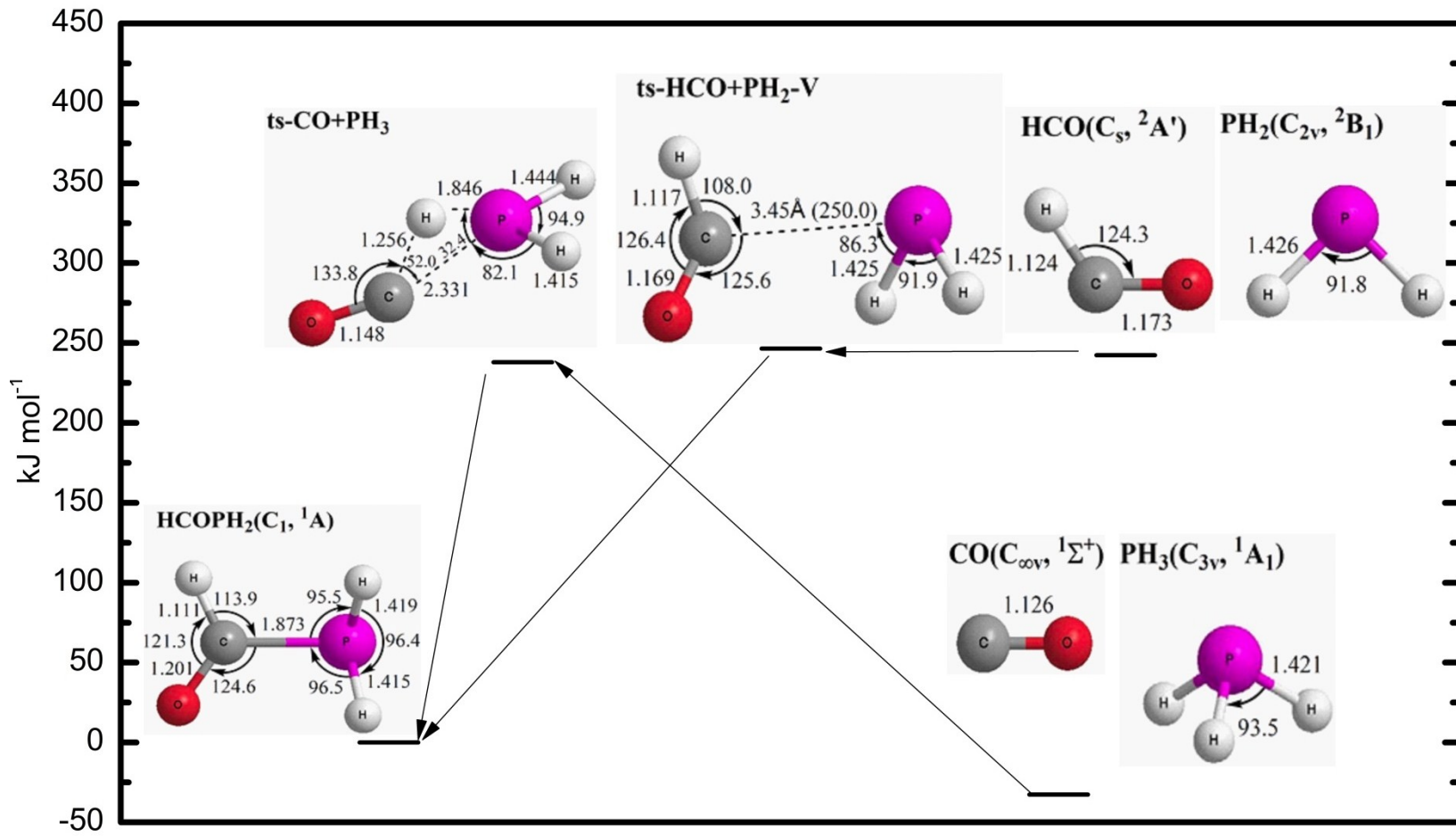


Fig S4 Calculated energies for formation pathways towards HCOPH_2

References

1. W. T. Reach, M. S. Kelley and J. Vaubaillon, *Icarus*, 2013, **226**, 777-797.
2. M. Agúndez, J. Cernicharo, L. Decin, P. Encrenaz and D. Teyssier, *The Astrophysical Journal Letters*, 2014, **790**, L27.
3. M. Agúndez, J. Cernicharo, J. R. Pardo, M. Guélin and T. G. Phillips, *Astronomy & Astrophysics*, 2008, **485**, L33-L36.
4. M. J. Abplanalp, A. Borsuk, B. M. Jones and R. I. Kaiser, *The Astrophysical Journal*, 2015, **814**, 45.
5. M. J. Abplanalp and R. I. Kaiser, *The Astrophysical Journal*, 2016, **827**, 132.
6. S. Góbi, L. Zhao, B. Xu, U. Ablikim, M. Ahmed and R. I. Kaiser, *Chemical Physics Letters*, 2018, **691**, 250-257.
7. S. Góbi, A. Bergantini and R. I. Kaiser, *The Astrophysical Journal*, 2017, **838**, 84.
8. B. M. Jones and R. I. Kaiser, *The journal of physical chemistry letters*, 2013, **4**, 1965–1971.
9. R. I. Kaiser, S. Maity and B. M. Jones, *Physical Chemistry Chemical Physics*, 2014, **16**, 3399-3424.
10. R. I. Kaiser and P. Maksyutenko, *The Journal of Physical Chemistry C*, 2015, **119**, 14653-14668.
11. S. Maity, R. I. Kaiser and B. M. Jones, *The Astrophysical Journal*, 2014, **789**, 36.
12. P. Maksyutenko, L. G. Muzangwa, B. M. Jones and R. I. Kaiser, *Physical Chemistry Chemical Physics*, 2015, **17**, 7514-7527.
13. M. Förstel, P. Maksyutenko, A. M. Mebel and R. I. Kaiser, *The Astrophysical Journal Letters*, 2016, **818**, L30.
14. M. Förstel, P. Maksyutenko, B. M. Jones, B. J. Sun, H. C. Lee, A. H. H. Chang and R. I. Kaiser, *The Astrophysical Journal*, 2016, **820**, 117.
15. Y. A. Tsegaw, S. Góbi, M. Förstel, P. Maksyutenko, W. Sander and R. I. Kaiser, *The Journal of Physical Chemistry A*, 2017, **121**, 7477-7493.
16. A. M. Turner, M. J. Abplanalp, S. Y. Chen, Y. T. Chen, A. H. H. Chang and R. I. Kaiser, *Physical Chemistry Chemical Physics*, 2015, **17**, 27281-27291.
17. M. Bouilloud, N. Fray, Y. Bénilan, H. Cottin, M.-C. Gazeau and A. Jolly, *Monthly Notices of the Royal Astronomical Society*, 2015, **451**, 2145-2160.
18. A. M. Turner, M. J. Abplanalp, T. J. Blair, R. Dayuha and R. I. Kaiser, *The Astrophysical Journal Supplement Series*, 2018, **234**, 6.
19. A. M. Turner, M. J. Abplanalp and R. I. Kaiser, *The Astrophysical Journal*, 2016, **819**, 97.
20. M. J. Abplanalp, S. Gozem, A. I. Krylov, C. N. Shingledecker, E. Herbst and R. I. Kaiser, *Proceedings of the National Academy of Sciences*, 2016, **113**, 7727-7732.
21. B. M. Jones, C. J. Bennett and R. I. Kaiser, *The Astrophysical Journal*, 2011, **734**, 78.
22. D. Drouin, A. R. Couture, D. Joly, X. Tastet, V. Aimez and R. Gauvin, *Scanning*, 2007, **29**, 92-101.
23. S. Góbi, M. Förstel, P. Maksyutenko and R. I. Kaiser, *The Astrophysical Journal*, 2017, **835**, 241.
24. M. J. Abplanalp and R. I. Kaiser, *The Astrophysical Journal*, 2017, **836**, 195.
25. M. Förstel, P. Maksyutenko, B. M. Jones, B.-J. Sun, A. H. H. Chang and R. I. Kaiser, *Chemical Communications*, 2015, **52**, 741-744.

26. M. Förstel, P. Maksyutenko, B. M. Jones, B.-J. Sun, S.-H. Chen, A. Chang, R. I. Kaiser and others, *ChemPhysChem*, 2015, **16**, 3139–3142.
27. M. Förstel, Y. A. Tsegaw, P. Maksyutenko, A. M. Mebel, W. Sander and R. I. Kaiser, *ChemPhysChem*, 2016, **17**, 2726–2735.
28. A. D. Becke, *The Journal of Chemical Physics*, 1992, **96**, 2155-2160.
29. A. D. Becke, *The Journal of Chemical Physics*, 1992, **97**, 9173-9177.
30. A. D. Becke, *The Journal of Chemical Physics*, 1993, **98**, 5648-5652.
31. C. Lee, W. Yang and R. G. Parr, *Physical Review B*, 1988, **37**, 785-789.
32. M. J. O. Deegan and P. J. Knowles, *Chemical Physics Letters*, 1994, **227**, 321-326.
33. C. Hampel, K. A. Peterson and H.-J. Werner, *Chemical Physics Letters*, 1992, **190**, 1-12.
34. P. J. Knowles, C. Hampel and H. J. Werner, *The Journal of Chemical Physics*, 1993, **99**, 5219-5227.
35. G. D. Purvis and R. J. Bartlett, *The Journal of Chemical Physics*, 1982, **76**, 1910-1918.
36. K. A. Peterson, D. E. Woon and T. H. Dunning, *The Journal of Chemical Physics*, 1994, **100**, 7410-7415.
37. M. J. Frisch, *GAUSSIAN 09, Revision D.01*, 2013.
38. O. Kostko, J. Zhou, B. J. Sun, J. S. Lie, A. H. H. Chang, R. I. Kaiser and M. Ahmed, *The Astrophysical Journal*, 2010, **717**, 674.
39. R. I. Kaiser, S. P. Krishtal, A. M. Mebel, O. Kostko and M. Ahmed, *The Astrophysical Journal*, 2012, **761**, 178.
40. R. I. Kaiser, P. Maksyutenko, C. Ennis, F. Zhang, X. Gu, S. P. Krishtal, A. M. Mebel, O. Kostko and M. Ahmed, *Faraday Discussions*, 2010, **147**, 429-478.
41. R. I. Kaiser, B. J. Sun, H. M. Lin, A. H. H. Chang, A. M. Mebel, O. Kostko and M. Ahmed, *The Astrophysical Journal*, 2010, **719**, 1884.
42. C. J. Bennett, C. S. Jamieson and R. I. Kaiser, *The Astrophysical Journal Supplement Series*, 2009, **182**, 1.
43. C. J. Bennett, C. S. Jamieson and R. I. Kaiser, *Physical Chemistry Chemical Physics*, 2010, **12**, 4032-4050.